PERIODICO di MINERALOGIA
established in 1930

Dipartimento
di Scienze della Terra
Sapienza Università di Roma

An International Journal of
Mineralogy, Crystallography, Geochemistry,
Ore Deposits, Petrology, Volcanology
and applied topics on Environment, Archaeometry and Cultural Heritage

Geochemistry signature, Sm-Nd and U-Pb isotopic data and age of dyke swarms in southwestern Jiroft, southern Iran

Hojatollah Jahangiri [1], Saeed Saadat [2,*], Seyed Ahmad Mazaheri [1], Mohammad Reza Heidarian Shahri [1], Petrus Le Roux [3], Mohammad Foudazi [4], Seyed Jafar Omrani [5]

[1] Department of Geology, Ferdowsi University of Mashhad, Mashhad, Iran

[2] Department of Geology and Petroleum Engineering, Mashhad Branch, Islamic Azad University, Mashhad, Iran

[3] Department of Geological Sciences, University of Cape Town, South Africa

[4] Department of Geology, Islamshar Branch, Islamic Azad University, Islamshahr-Tehran, Iran

[5] Geological Survey and Mineral Explorations of Iran, Tehran 131851494, Iran

ARTICLE INFO

Submitted: June 2020
Accepted: February 2021
Available on line: July 2021

* Corresponding author:
saeed.saadat@colorado.edu

Doi: 10.13133/2239-1002/17500

How to cite this article:
Jahangiri H. et al. (2021)
Period. Mineral. 90, 289-306

ABSTRACT

Numerous NW-SE trending dykes outcrop in south west of Jiroft, Southern Iran. These dykes are mainly composed of diorite, quartz diorite, gabbro-diorite, and gabbro. Plagioclases in the dyke swarm have composition ranging from $An_{99.5}Ab_{0.5}$ in cores, to $An_{17}Ab_{78}Or_5$ in rims, and compositional variation with $En_{42-49}Wo_{39-40}Fs_{11-18}$ in clinopyroxene plots across the augite field boundary. These rocks show strongly metaluminous signatures and tholeiitic affinity. Studied rocks display La_N/Lu_N=0.68-2.19 and Eu_N/Eu^*=1.63-1.92 with nearly flat heavy rare earth element (HREE). The U-Pb age dating of zircons from a dyke yielded 36.07±0.07 Ma indicating Eocene crystallization age, to an age of 783.85±1.98 Ma, indicating this dyke has zircon xenocrysts inherited. The initial $^{87}Sr/^{86}Sr$ and $^{143}Nd/^{144}Nd$ isotopic composition of studied swarm dykes are 0.705287±0.000009 and 0.512833±0.00001 respectively. Geochemical data show transitional geochemical characteristics between normal mid-ocean ridge basalt and island arc tholeiites. Geochemical and isotopic data indicate they formed by around 15% melting of a spinel-mantle source metasomatized by fluids derived from subducted oceanic slab.

Keywords: swarm dyke; U-Pb geochronology; geochemistry; Jiroft; Iran.

INTRODUCTION

Dykes swarms represent direct evidence for magma generation and understanding geodynamic processes that occur from Archaean to recent, and mark recurring episodes of continental extension (e.g. Kerr et al., 2000; Ernst and Buchan, 2001; Bernard and Daniel, 1999) in a variety of tectonic settings such as mid-ocean spreading ridges (Robinson et al., 2008), back-arc, and post-collisional tectonic regimes (Taylor and Martinez, 2003; Xu et al., 2012). The fast emplacement, orientation, morphology, composition, and age, make swarm dykes valuable source to understand the relationships between magmatic and tectonic processes (e.g. Bryan and Ferrari, 2013; Bryan and Ernst, 2008; Ernst, 2014). They are also known to host many economic deposits of PGE and Au, base metals, diamonds, Ni-Cr-Co (e.g. Peck et al., 2001; James et al., 2002; Iljina and Hanski, 2005).

Many swarm dykes have been identified in various structural zones of Iran (e.g. Bazoobandi et al., 2015; Aliani and Daraeezadeh, 2018). In the northern margin of the Southern Sanandaj-Sirjan zone, in the Esfandagh-sabzevaran subzone, a large number of mafic to intermediate dykes has outcropped (Figure 1). The distribution patterns of these dykes represent specific tensile conditions at the time of their formation.

This work presents an integrated field, petrographic, geochemical and Sr-Nd-Pb isotope study of intermediate to mafic dykes from the southwest of Jiroft area, southeastern part of Sanandaj-Sirjan zone, which has not yet been reported by earlier researchers (Figure 1). This project aims to investigate the geochemical, isotopic characteristics, and age determination of the swarm dykes, for better understanding the petrogenesis and tectonic setting of these rocks.

BACKGROUND GEOLOGY

The Zagros Mountains as a part of Alpine-Himalayan Orogenic Belt are subdivided into the Zagros Fold and Thrust Belt, the Zagros Suture Zone, the Sanandaj-Sirjan Zone, and the Late Cretaceous ophiolite belt (Mohajjel et al., 2003) (Figure 1).

The formation of this belt is related to the collision of the Central Iran with Arabian Plates and closure of the Neotethys Ocean (e.g. Alavi, 2004; Berberian and King, 1981; Mohajjel et al., 2003; Sadeghi and Yassaghi, 2015). Timing of collision is still under discussion but the most significant suggestion is Late Cretaceous to Miocene (Berberian and Berberian, 1981), uppermost Pliocene (Stöcklin, 1968, 1977) and late Eocene to Oligocene (e.g. Agard et al., 2005, 2011; Vincent et al., 2005; Ballato et al., 2010). The Sanandaj-Sirjan zone (SSZ) is a region of polyphase deformation on the southwestern margin of Eurasia. The SSZ is characterized by a metasedimentary and metavolcanic sequence of Mesozoic age riddled by intrusive bodies of the Mesozoic to Cenozoic time span (e.g., Agard et al., 2011; Mohajjel and Fergusson, 2014; Mohajjel et al., 2003).

In the study area, which is located in southeastern part of SSZ, crystal vitric tuff is the oldest rock unit that has outcropped in the eastern part (Figure 1). The texture of these rocks is clastic and the main forming minerals are quartz and plagioclase. The volcano-sedimentary unit is mainly composed of basaltic pillow and massive lava flows associated with pelagic sediment as intercalation. This unit belongs to deep oceanic basin and it is associated with ophiolitic rocks and colored mélange complex around the study area. The pillow and massive lava flows unit are mainly basalt and some of them slightly tend to be andesitic basalt. The main texture of these rocks is porphyry. The pelagic sediments involve mudstone, silty mudstone, tuffaceous limestone, micritic limestone, shale, and banded radiolarian chert (Figure 1). The duration and time of oceanic processes is Early Middle Jurassic-Early Cretaceous concluded using biostratigraphy interpretation of the radiolarian chert (Jahangiri et al., 2020). Jurassic series ended by volcanoclastic rocks contain rhyodacitic tuff, marly and sandy tuff and sandstone. Intrusive rocks as gabbro and diorite in composition have outcropped in northeastern part in this area (Figure 1).

Dyke swarms have been emplaced into the Jurassic-Cretaceous units. These long and parallel dykes are vertical with northwest to southeast trend. Some of these dykes were injected along pre-existing steeply-dipping faults striking at NW-SE trend (Figure 1).

METHODS

The compositions of rock-forming minerals were analyzed using a CAMECA SX 100 electron microprobe at the laboratory of University of Strasbourg in France with four wavelength-dispersive spectrometers (WDS). Silicate minerals were examined using 15 kV accelerating voltage, 10 nA beam current, and 8 μm beam diameter. The sensitivity of the device depends on the element and the matrix and varies from a few 10 ppm to a few 100 ppm. Plagioclase, clinopyroxene, and prehnite were determined by Electron microprobe analyses (Table 1).

The six least-altered samples were selected for major and trace element analyses. Major, trace and REEs were determined by inductively coupled plasma atomic emission spectrometry (ICP-AES), and inductively-coupled plasma mass spectrometry (ICP-MS) in Als loughrea Analytical Laboratories Ltd. (Galway, Irland) (Table 2). The ICP-AES analysis was read on ICP-OES 5110 (procedure ME-MS61) and the ICP-MS was read on ICP-MS7700 (procedure ME-MS81). Some detection limits for this method are following: Nb (0.005-500 ppm), Rb (0.01-10000 ppm), Ta (0.01-500 ppm), Th (0.004-10000 ppm), Zr (0.1-500 ppm), Y (0.01-500 ppm), Eu (0.02-1000 ppm), Ho (0.01-1000 ppm), Lu (0.01-1000 ppm), Nd (0.1-10000 ppm), Sm (0.03-1000 ppm), Tm (0.01-1000 ppm) and Yb (0.03-1000 ppm).

Whole rock samples (20 Kg) was crushed using jaw crushers, then sieved to obtain the size fraction above ~300 μm. Sample was washed with water to remove dust. After washing and drying, magnetic minerals, such as magnetite, were removed with a Franz magnetic separator. Then 30 Zircon grains were handpicked from one selected sample under a binocular microscope, using standard mineral-separation techniques at Geological Survey and Mineral Exploration of Iran (GSI). All zircon grains were mounted on adhesive tape then enclosed in epoxy resin discs and polished to about half of their diameter. All zircon grains were investigated by cathodoluminescence (CL) to highlight zoning and possible inherited cores. U-Pb isotopic analyses of zircons were conducted by laser ablation inductively coupled plasma-mass spectrometry

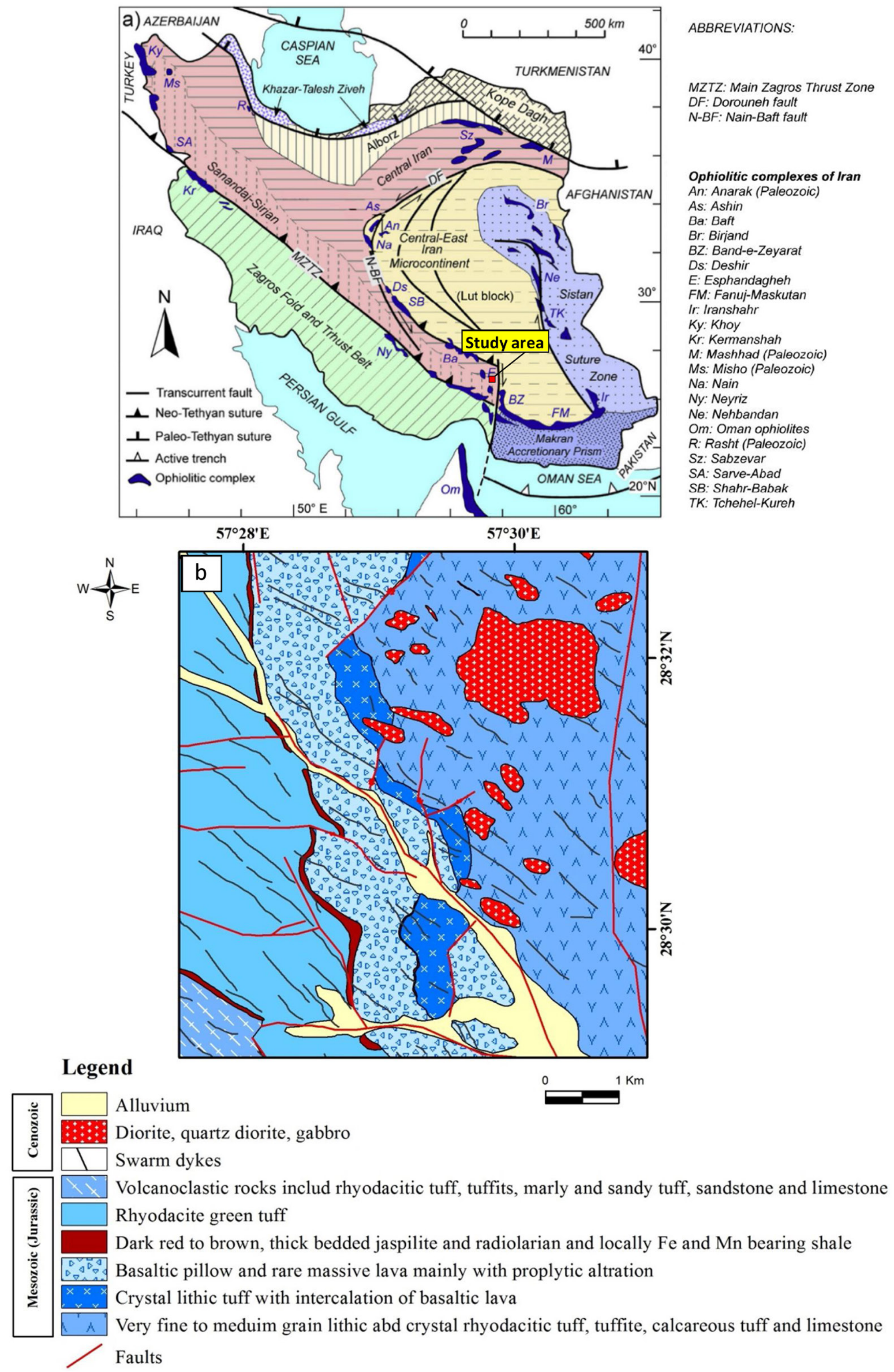

Figure 1. a) Geological map of Iran. Ophiolites and major tectonic units are shown (Pirnia et al., 2020), b) Simplified geological map of study area (modified after Aghazadeh and Ojaghi, 2009).

Table 1. Mineral chemistry of plagioclase, pyroxene and prehnite.

Mineral	Plagioclase		
Sample	Qr-95-3	Qr.285	
No.	2	1(core)	2(rim)
SiO_2	65.95	41.69	61.89
Al_2O_3	19.23	18.49	22.74
FeO	0.23	6.88	0.41
CaO	3.49	25.50	3.32
Na_2O	10.12	0.06	8.39
K_2O	0.16	0.00	0.90
Total	99.17	92.62	97.63
Number of ions on basis of 32 oxygens			
Si	2.94	2.16	2.81
Al	1.01	1.13	1.22
Fe	0.01	0.30	0.02
Ca	0.17	1.41	0.17
Na	0.87	0.01	0.74
K	0.01	0.00	0.05
Or	0.83	0.00	5.48
Ab	83.27	0.41	77.59
An	15.90	99.59	16.95

Mineral	Pyroxene		
Sample	Qr-95-3		Qr.285
No.	5	2	4
SiO_2	51.51	52.40	50.08
TiO_2	0.26	0.20	0.37
Al_2O_3	1.88	1.93	2.26
Cr_2O_3	0.11	0.55	0.12
FeO	10.90	6.99	11.42
MnO	0.29	0.22	0.30
MgO	14.66	17.17	15.64
CaO	19.01	19.19	18.07
Na_2O	0.19	0.15	0.22
Total	98.81	98.79	98.46
Si	1.94	1.95	1.89
Ti	0.01	0.01	0.01
Al	0.08	0.08	0.10
Cr	0.00	0.02	0.01
Fe	0.32	0.21	0.25
Mn	0.01	0.01	0.01
Mg	0.82	0.95	0.88
Ca	0.77	0.76	0.73
Na	0.01	0.01	0.02
En	42.50	49.22	44.61
Wo	39.68	39.53	37.11
Fs	17.82	11.26	18.28

Mineral	Prehnite		
Sample	Qr.95.3		
No.	Prhe.P:14	Prhe.P:15	Prhe.P:16
SiO_2	44.68	45.97	44.67
TiO_2	0.00	0.00	0.01
Al_2O_3	22.74	22.66	23.55
FeO	4.11	3.78	3.22
MnO	0.03	0.00	0.02
MgO	0.24	0.04	0.12
CaO	24.90	24.70	25.39
Na_2O	0.11	0.01	0.07
Total	96.87	97.24	97.09
Cations			
Si	6.14	6.25	6.10
Al total	3.68	3.63	3.79
Fe	0.47	0.43	0.37
Mg	0.05	0.01	0.02
Ca	3.67	3.607	3.72
Na	0.03	0.003	0.02
OH *	4.00	4.00	4.00
Total	18.04	17.93	18.01

(LA ICP-MS) at the ETH Zurich. ICP-MS ELAN 6000 (Perkin Elmer Corp., Norwalk, USA) Power 1.1±1.6 kW Vacuum 1.35 10^{-5} torr (0.75 mm cone orifice, Al-cone), Carrier gas flow (helium) 1.2 l/min, Carrier gas flow (argon) 1.1 l/min, Auxiliary gas flow 0.85 l/min, Cool gas flow 16 l/min Quadrupole settling time 3 ms Detector Mode Pulse counting and analogue Dwell time/isotope 10 ms Points/mass 1. All zircon grain and 14 standard zircon samples were analyzed by laboratory.

For radiogenic isotopes, approximately 50 mg of whole rock powder was dissolved in a 4:1 HF/HNO_3 acid mixture in sealed Savillex beakers on a hot plate for 48 hours, and the solution was then split for determination of both concentration data (Rb, Sr, Nd and Sm), and Sr and Nd isotope ratios. The Sr and Nd fractions for isotope analysis were isolated employing sequential column chemistry (after Mikova and Denkova, 2007; Pin and Zalduegui, 1997). The Sr and Nd isotope data were obtained using a Nu Plasma HR mass spectrometer equipped with a DSN-100 nebulizer. All Sr isotope data were referenced to a value of 0.710255 for the bracketing analyses of NIST SRM987. Sr isotope data were corrected for Rb interference using the measured signal for ^{85}Rb and the natural ^{85}Rb/^{87}Rb ratio, while instrumental mass fractionation was addressed using the exponential law and a ^{86}Sr/^{88}Sr value of 0.1194. The Nd isotope values were normalized to a value of 0.512115 for bracketing analyses of JNdi-1, (Based on Tanaka et al, 2000).

FIELD OBSERVATION AND PETROGRAPHY

Very long and parallel swarm dykes with northwest to southeast trend have intruded old units such as pelagic sediment and pillow and massive lava flows. The length of the dykes varies from several meters to more than a kilometer when the width varies from a few meters up to 20m. The walls of dykes are smooth and show a higher morphology than its host-rock (Figure 2). There are old mining workplace adjacent to swarm dykes, and mineralized zone consisting

Table 2. Whole-rock major and trace element compositions of swarm dykes. Oxide (wt%) and elements (ppm).

Sample	Gr.285	Tr.260	Qr.3	Gr.319	Qr-13	Qr.22
SiO_2	55.3	54.9	55.7	55.7	47.6	47.9
Al_2O_3	14.75	15.05	14.55	14.90	15.65	15.50
Fe_2O_3	11.40	10.85	11.30	11.20	10.55	10.70
CaO	7.51	8.47	7.03	7.68	10.90	10.50
MgO	3.78	3.72	3.84	3.39	7.35	6.88
Na_2O	3.03	3.23	3.22	2.97	2.62	2.91
K_2O	1.05	0.48	1.08	0.93	0.18	0.56
TiO_2	0.81	0.8	0.82	0.72	1.04	1.01
MnO	0.18	0.15	0.17	0.17	0.18	0.19
P_2O_5	0.13	0.12	0.15	0.12	0.08	0.08
LOI	2.51	2.97	2.33	2.72	2.91	2.68
Total	100.45	100.74	100.19	100.50	99.06	98.91
V	345	327	365	338	302	331
Cr	40	50	40	20	220	160
Ga	17.6	18.8	17.7	17.7	15.7	16.3
Rb	25.4	7.3	26	22.6	2.5	12.2
Sr	282.0	112.5	269.0	251.0	149.0	224.0
Y	20.9	21.4	21.5	21.3	23.9	23.6
Zr	55	69	59	60	56	51
Nb	1.4	1.9	1.3	1.3	1.1	1.0
Cs	0.46	0.11	0.42	0.34	0.26	1.81
Ba	312.0	131.5	295.0	220.0	73.8	102.5
La	5.7	7.6	5.8	5.9	2.5	2.7
Ce	11.9	14.2	11.7	11.8	6.7	6.6
Pr	1.56	1.85	1.56	1.57	1.13	1.06
Nd	7.3	9.0	7.6	7.4	6.2	6.1
Sm	2.16	2.46	2.36	2.23	2.19	2.00
Eu	0.64	0.80	0.74	0.71	0.80	0.84
Gd	2.94	3.11	3.02	3.20	3.29	3.04
Tb	0.49	0.54	0.49	0.51	0.61	0.59
Dy	3.31	3.43	3.35	3.25	4.05	3.94
Ho	0.74	0.85	0.79	0.77	0.93	0.91
Er	2.14	2.30	2.30	2.21	2.54	2.48
Tm	0.36	0.37	0.34	0.34	0.40	0.39
Yb	2.27	2.49	2.31	2.26	2.68	2.33
Lu	0.35	0.36	0.36	0.36	0.38	0.35
Hf	1.6	2.1	1.8	2.0	1.5	1.4
Ta	0.2	0.2	0.2	0.2	0.1	0.1
Th	1.76	2.62	1.78	1.87	0.32	0.34
U	0.55	0.72	0.51	0.54	0.11	0.09

hematite, goethite, sericite, silica has formed in margin of some swarm dykes (Figure 2).

The chemical compositions of these dykes are diorite, quartz diorite, gabbro-diorite, and gabbro. These dikes show a variety of textures that include medium to microgranular, ophitic or subophitic, porphyry, intercertal, and intergranular textures (Figure 3).

The most important minerals are the subhedral plagioclase (45-60 vol%) and euhedral to sub-euhedral clinopyroxene (35-45 vol%), with varying content of accessory minerals, such as hornblende and quartz. Clinopyroxene is the most important mafic mineral of this rock unit. Amphibole forms up to 15% and can be divided into two generations: primary amphibole is brownish and the secondary amphibole (tremolite or actinolite) is bluish-green.

Some of plagioclases (50-55%) altered into chlorite, calcite, sericite, prehnite and albite and some of clinopyroxene altered into chlorite, tremolite and actinolite. The hornblende is locally altered into chlorite and biotite.

RESULTS

Mineral chemistry

Plagioclase

Plagioclase as phenocryst and groundmass phases is the most abundant mineral in these dykes (Figure 4). The chemical compositions of representative plagioclase are listed in Table 1. Plagioclases in the dyke swarm has composition ranging from $An_{99.5}Ab_{0.5}$ in cores to $An_{17}Ab_{78}Or_5$ in rims of sample named QR95-285 and ranging from $An_{15}Ab_{84}Or_1$ to $An_{17}Ab_{82}Or_1$ in sample named QR95-3 (Table 1).

Pyroxene

Representative electron microprobe analyses of fresh clinopyroxene crystals are shown in Table 1. Clinopyroxenes have 0.2-0.37 wt% TiO_2, 1.8-2.26 wt% Al_2O_3, 14.66-17.17 wt% MgO, 18-19.2 wt% CaO and 7-10.9 wt% FeO (Table 1). The clinopyroxene phenocrysts (Figure 4) show compositional variation with $En_{42-49}Wo_{39.5-39.7}$ Fs_{11-18} (in sample QR95-3) and $En_{45}Wo_{37}Fs_{18}$ (in sample QR95-285).

Prehnite

Prehnite occurs as alteration product of plagioclase. Formation of hydrothermal prehnite occurs in presence of alkali chloride hot waters (>200 °C) with neutral to slightly alkaline pH and low dissolved CO_2 (Wheeler et al., 2001). Prehnite from the studied dykes, as showm in Table 1, displays minor compositional variability mainly involving Fe and Al. The occurrence of prehnite in a hydrothermal system indicate that degassing of the hydrothermal fluid in CO_2 occurred prior to deposition (Wheeler et al., 2001).

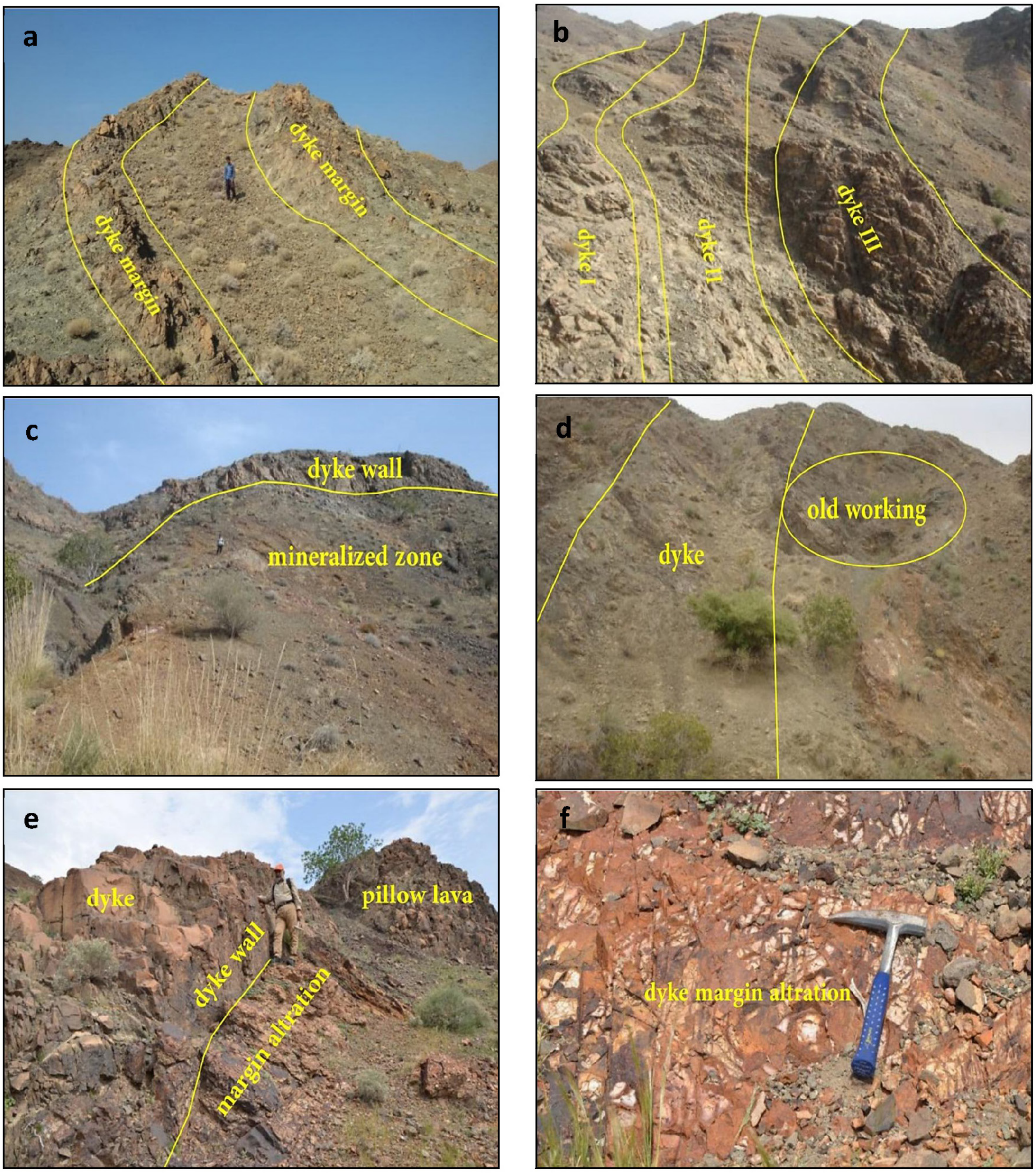

Figure 2. General view of swarm dykes: a) Swarm dyke with a cold margin, b) Set of parallel swarm dykes, c) A view of the injection of swarm dyke in the mineralized zone, d) Old mining workplace adjacent to swam dyke, e) Formation of hematite, goethite, sericite, silicic and argillic alteration in margin of swam dyke, f) Mineralized stock work zone with hematite, gothic, sericite, silica, and argillic alterations.

Whole-rock geochemistry

Major element

The results of major elements composition are shown in Table 2. Based on the chemical classification diagram (Cox, 1979) and Middlemost (1994), these rocks plot in gabbro to diorite field (Figure 5). Samples are met-aluminous in Shand (1943) diagram and show tholeiitic affinity in Miyashiro (1974) plot (Figure 5).

Trace and rare earth element

The trace element concentration of studied samples is presented in Table 2. The chondrite-normalized (McDonough and Sun, 1995) REE samples are characterized by relatively flat heavy REEs (Figure 6). In chondrites normalized REEs pattern, all samples are about 10 times richer in REEs than chondrites. There is a minor enrichment in light rare earth elements (LREEs)

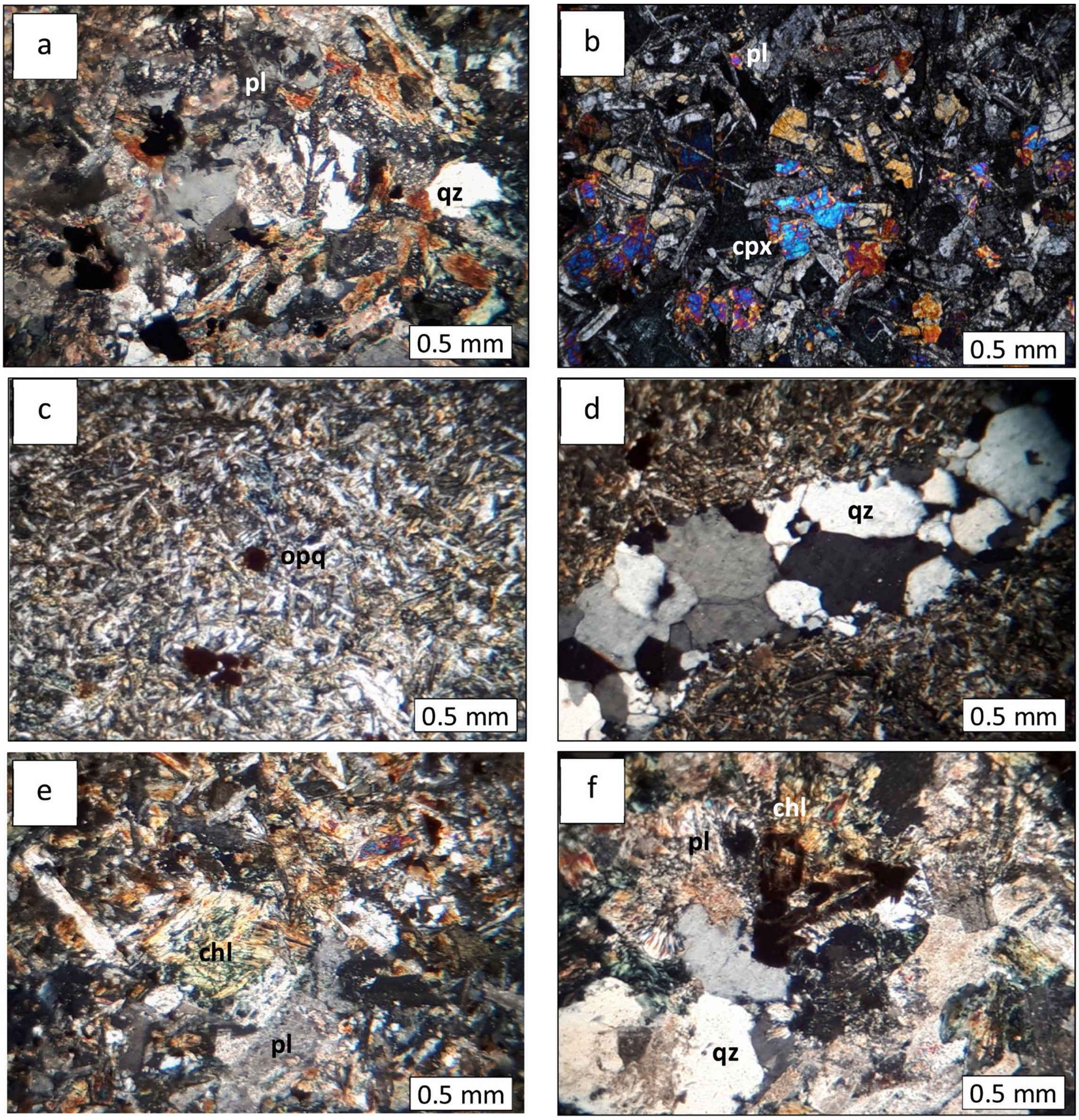

Figure 3. Microphotographs of the swarm dykes samples: a) Granular texture in monozodiorite, b) Sub ophitic and inter granular texture in diorite, c) Variolitic texture in the outer part of the dyke (cold margin) with albite and chlorite alteration, d) Quartz veinlet in dykes, e) Sericite and chlorite alteration, f) Uralitization in clinopyroxene and chloritization in plagioclase. (Crossed nicols; pl: plagioclase, cpx: clinopyroxene, qz: quartz, opq: opaque minerals, chl: chlorite). Abrasive from Whitney and Evans (2010).

for some samples with $(La/Yb)_N$ values 0.63-2.06 (Figure 6). These rocks display La_N/Lu_N=0.68-2.19 and Eu_N/Eu^*=0.78-1.04. Distribution of REE values reflects nearly flat heavy rare earth elements (HREEs) on the normalized REE patterns compared to chondrite values (Figure 6).

All samples are characterized by Nb and Ti depletion in Primitive Mantle normalized (Sun and McDonough, 1989) and Chondrite normalized (McDonough and Sun, 1995) spider diagrams, with La_N/Sm_N=0.74-2 and La_N/Sm_N=0.72-1.94 respectively (Figure 6).

The REE pattern of swarm dykes has been compared with mafic dykes from Kermanshah in northwestern part of the Zagros main thrust. N-MORB-normalized multi-element plots indicate nearly flat patterns for HFSE and enrichment in LILE; patterns of incompatible trace elements demonstrate an island arc (IAT) affinity for these rocks.

Zircon U-Pb Geochronology

One sample was selected for zircon U-Pb geochronology

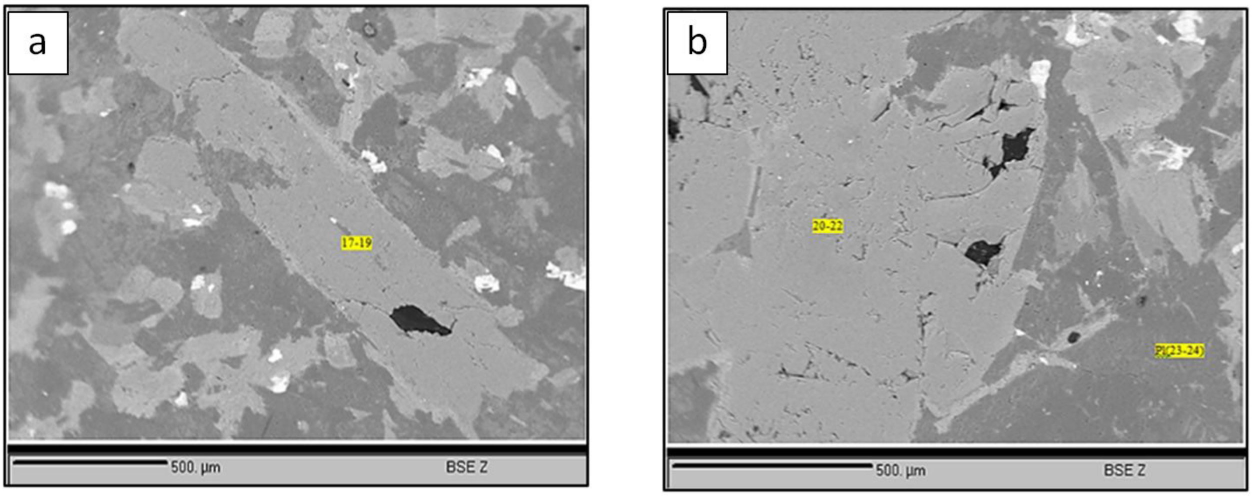

Figure 4. Back scattered electron images of (a) plagioclase and (b) pyroxenes.

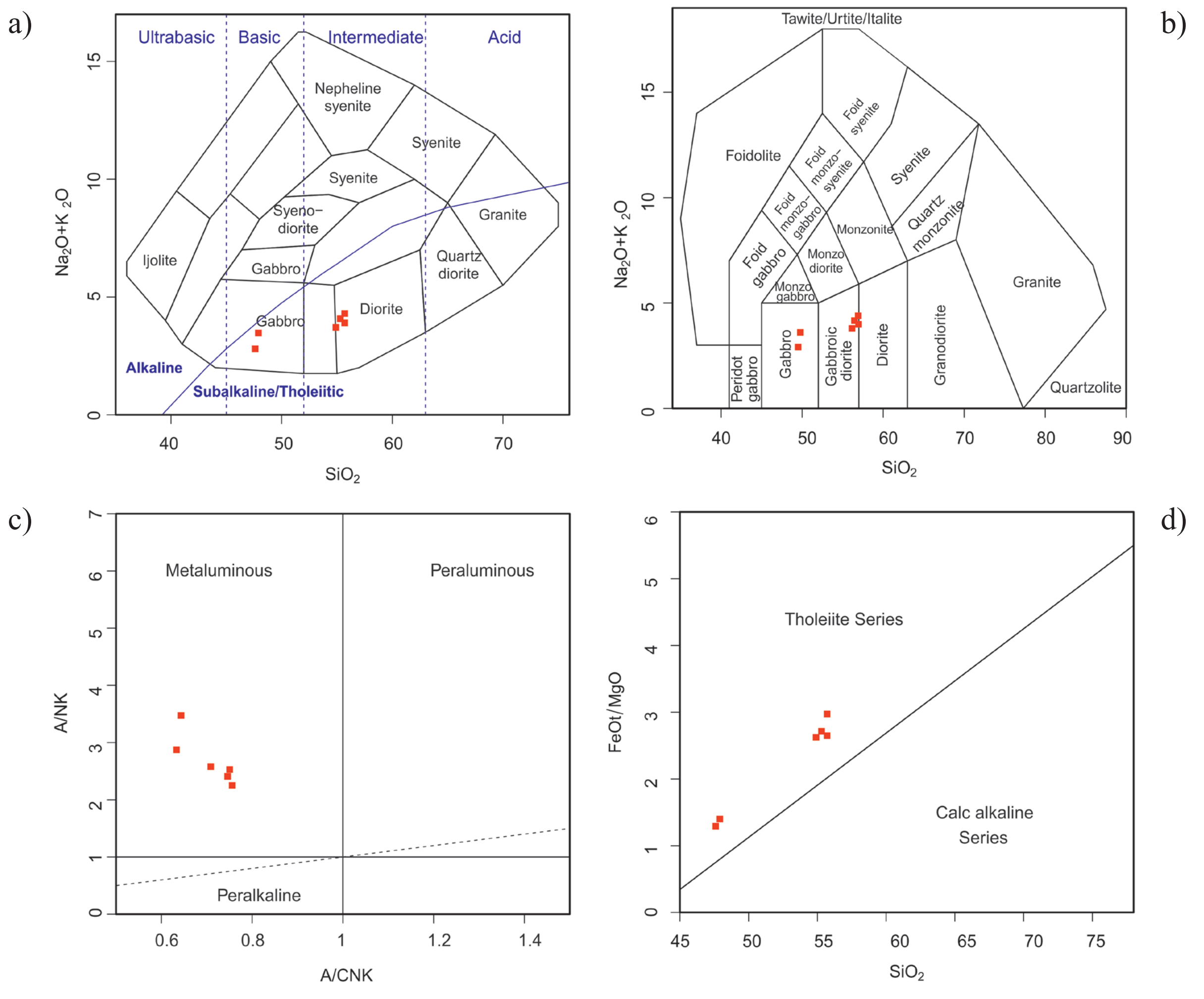

Figure 5. Chemical classification of the swarm dykes on a) Na_2O+K_2O/SiO_2 diagram (Cox, 1979), b) Na_2O+K_2O/SiO_2 diagram (Middlemost, 1994), c) Most of samples plot in Metaluminous environment on Shand (1943) diagram, d) Samples plot in tholeiites series in FeOt/MgO versus SiO_2 diagram (Miyashiro, 1974).

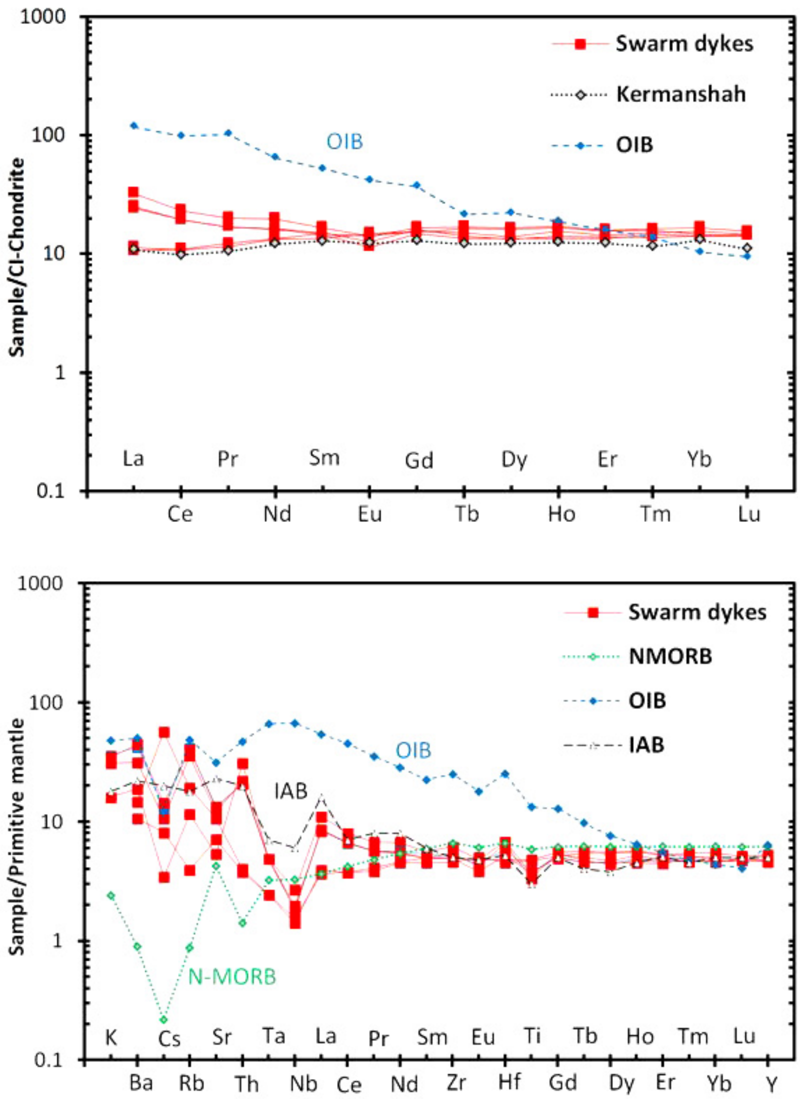

Figure 6. Trace element and REE variations of the swarm dykes comparing with OIB, IAB, N-MORB, and average composition of mafic dykes from Kermanshah (Aliani and Daraeezadeh, 2018). Normalization values from Sun and McDonough (1989) and McDonough and Sun (1995).

and 30 zircon were analyzed for this sample (Table 3). The zircon crystals, with a maximum size close to 150µm, are automorphic to sub-idiomorphic, and display a well-developed oscillatory zoning indicative of growth under magmatic conditions (Koschek, 1993; Wu et al., 2007; Zhai et al., 2009; Buick et al., 2008). Uranium concentration ranges from 23 to 601 ppm and Th varies from 40 to 1104 ppm. The ratio of U/Th in metamorphic zircon grains is usually greater than 5 to 10, and in the magmatic zircon grains, it is less than 5 (Rubatto, 2002: Chen et al., 2007; Belousova et al., 2002). This feature is associated with an isotopic closing temperature (up to 900 ºC), which allows to accept the data of U-Pb as the representative of the dyke crystallization age (Cherniak and Watson, 2000). In the study area this ratio, below 5, is regarded as being derived from magmatic crystallization.

The combination of cathodoluminescence (CL) imaging and U-Pb dating determined a number of “inherited” zircons (Figure 7). Cathodoluminescence image of these zircon grain shows rounded and broken crystals, which are inherited zircon with magmatic source.

The distribution of zircon ages implies that the zircons in the dyke yielded different ages. There are two populations in the spots. Main population contain 20 analyzed spots that define a $^{206}Pb/^{238}U$ age in Cenozoic time with the 36.076±0.073 Ma interpreted as the crystallization age (Figure 8).

U concentrations of these zircons vary from 72 to 584

Table 3. Zircon U-Pb isotopic data for selected sample from swarm dykes in the study area.

Sample	Th (ppm)	U (ppm)	U/Th	$^{207}Pb/^{235}U$	± 2s	$^{206}Pb/^{238}U$	± 2s	$^{208}Pb/^{232}U$	± 2s	Final age $^{206}Pb/^{238}U$	± 2s
Ja-Fine - 1	197	167	1.271	1.169	0.042	0.127	0.0024	0.0401	0.0025	770	14
Ja-Fine - 4	106.7	75.6	1.41	0.069	0.011	0.01	0.00017	0.0031	0.0004	63.05	1.1
Ja-Fine - 5	220.7	187.3	1.178	0.0591	0.0069	0.008	0.00013	0.0021	0.0002	50.9	0.84
Ja-Fine - 6	193	282	0.775	0.054	0.011	0.007	0.00017	0.002	0.00027	42.8	1.1
Ja-Fine - 9	746	371	2.01	0.0324	0.0028	0.005	0.000067	0.0015	0.00017	30.16	0.43
Ja-Fine - 10	439	356	1.227	0.0405	0.0042	0.006	0.000083	0.0018	0.00014	37.99	0.53
Ja-Fine - 12	173	32.7	4.91	1.73	0.052	0.173	0.003	0.0502	0.0034	1027	16
Ja-Fine - 13	475	410	1.177	0.0334	0.0037	0.005	0.000072	0.0015	0.00013	30.9	0.46
Ja-Fine - 14	365	183.2	1.986	1.082	0.035	0.124	0.0017	0.0358	0.0022	751.3	9.9
Ja-Fine - 15	215	218.1	0.963	0.776	0.03	0.093	0.0023	0.0281	0.0016	573	13
Ja-Fine - 16	987	601	1.635	1.257	0.017	0.136	0.0017	0.0404	0.0021	823.5	9.4
Ja-Fine - 17	773	383	2.163	0.0521	0.0039	0.008	0.00011	0.0023	0.00018	50.07	0.69
Ja-Fine - 18	419	197	2.186	1.37	0.031	0.145	0.0019	0.0396	0.0022	873.7	11
Ja-Fine - 21	329	380	0.87	0.0654	0.0061	0.009	0.00015	0.0029	0.00021	59.87	0.95
Ja-Fine - 23	457	465	1	0.0501	0.0059	0.006	0.0001	0.0023	0.00019	41.34	0.66
Ja-Fine - 25	386	430	0.8919	0.07	0.0057	0.01	0.00014	0.0031	0.00022	65.07	0.9
Ja-Fine - 28	40.1	36.3	1.118	1.15	0.079	0.126	0.0025	0.0381	0.0027	762	14
Ja-Fine - 29	70.9	71.7	0.988	0.086	0.019	0.007	0.00016	0.0031	0.00046	42.42	1
Ja-Fine - 30	53.5	23	2.257	1.27	0.082	0.136	0.0034	0.041	0.0031	824	19
Ja-Fine - 33	129	114.6	1.151	0.0274	0.0079	0.003	0.000082	0.001	0.00019	20.71	0.52
Ja-Fine - 34	266	249	1.069	0.0309	0.0041	0.005	0.000073	0.0014	0.00014	28.98	0.47
Ja-Fine - 35	1104	491	2.243	0.0238	0.0028	0.003	0.000056	0.001	0.00009	21.36	0.36
Ja-Fine - 38	480	221	2.207	0.26	0.16	0.007	0.0012	0.0128	0.008	47.1	7.2
Ja-Fine - 39	797	526	1.506	0.0682	0.0038	0.009	0.00015	0.0029	0.00019	60.88	0.98
Ja-Fine - 40	525	142	3.69	1.411	0.077	0.118	0.0024	0.0608	0.0058	721	14
Ja-Fine - 41	2530	451	5.64	0.0506	0.0024	0.007	0.00011	0.0024	0.00021	45.9	0.71
Ja-Fine - 42	133.2	115.2	1.158	0.065	0.012	0.007	0.00014	0.0029	0.00037	45.69	0.9
Ja-Fine - 44	979	584	1.662	0.0631	0.0036	0.008	0.00012	0.0029	0.00021	53.85	0.76
Ja-Fine - 47	158.2	147.9	1.084	0.047	0.0079	0.007	0.00012	0.0022	0.00024	41.84	0.8

ppm, and Th abundances are 71 to 1104 ppm, with the U/Th ratio of 0.8-2.2 (Table 3). The second population involve older zircon ages ranging from 573 to 1027 Ma. Weighted mean $^{206}Pb/^{238}U$ age of Precambrian zircon grains is 783±1.98 Ma (Figure 8). U concentrations of these zircons vary from 23 to 601 ppm, and Th abundances are 40 to 987 ppm, with the U/Th ratio of 0.9-4.9 (Table 3).

Rb-Sr and Sm-Nd isotopic Data

Rb-Sr and Sm-Nd isotopic data from one sample of swarm dyke are presented in Table 4. The $^{87}Sr/^{86}Sr$ and $^{143}Nd/^{144}Nd$ initial ratios for selected sample are 0.705287 and 0.512833, respectively. Recalculated to the age of crystallization, the εNd values for this sample is +4.7 (Table 4). The $^{143}Nd/^{144}Nd_i$ versus $^{87}Sr/^{86}Sr_i$ diagram is similar to the common field of MORB (Figure 9). These values are higher than Bulk Earth $^{87}Sr/^{86}Sr$ and $^{143}Nd/^{144}Nd$ ratios.

DISCUSSION AND CONCLUSION

Crustal Contamination

During dyke emplacement into crustal levels, different degrees of crustal contamination may occur in mantle-derived magmas (Mohr, 1987). Crustal xenoliths or wall-rocks have not been observed in studied dykes, but the existence of inherited Proterozoic zircons in these dykes

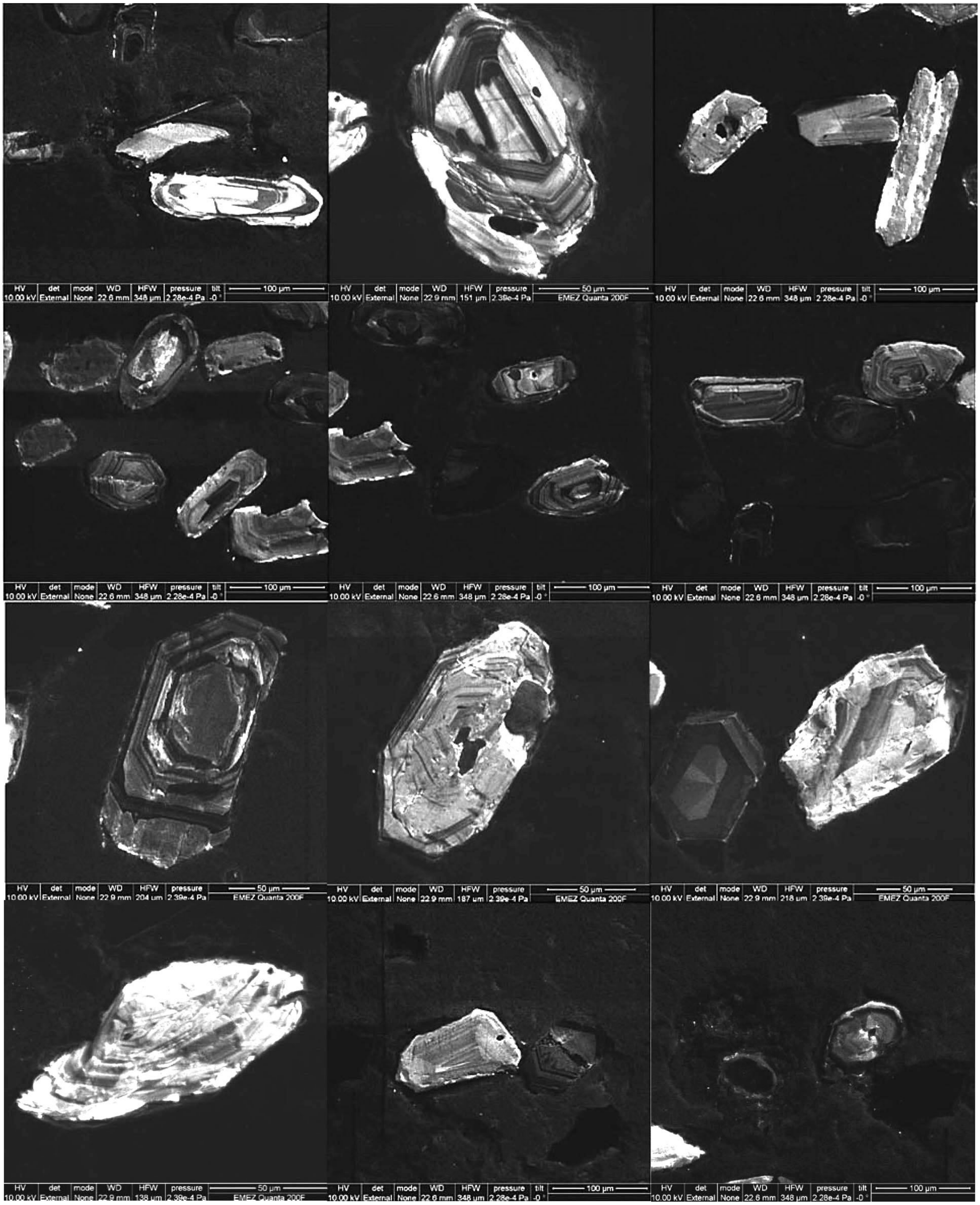

Figure 7. Cathodoluminescence images of some representative zircon grains from studied dykes.

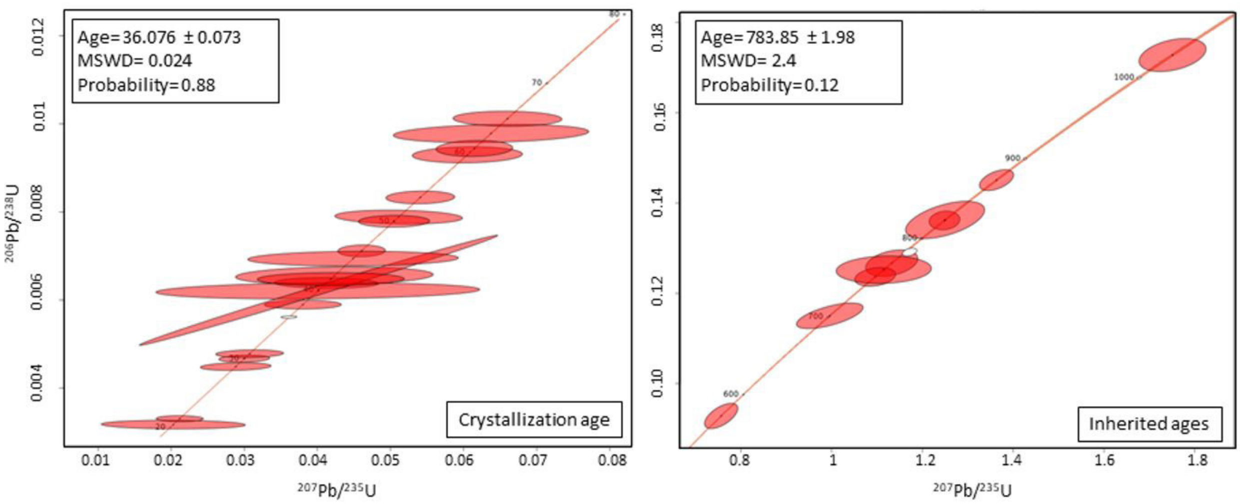

Figure 8. Zircon LA- ICP-MS U-Pb concordia diagrams for swarm dykes in the study area.

Table 4. Rb-Sr and Sm-Nd isotopic data from the selected swarm dyke in the study area.

Sample	Age (Ma)	Sr (ppm)	Rb (ppm)	$^{87}Sr/^{86}Sr$ measured	$^{87}Sr/^{86}Sr$ initial	Nd (ppm)	Sm (ppm)	$^{143}Nd/^{144}Nd$ initial	$^{143}Nd/^{144}Nd$ initial	εNd
Gr-95-285	36	282	25.4	0.705420	0.705287	7.3	2.16	0.512875	0.512833	+4.7

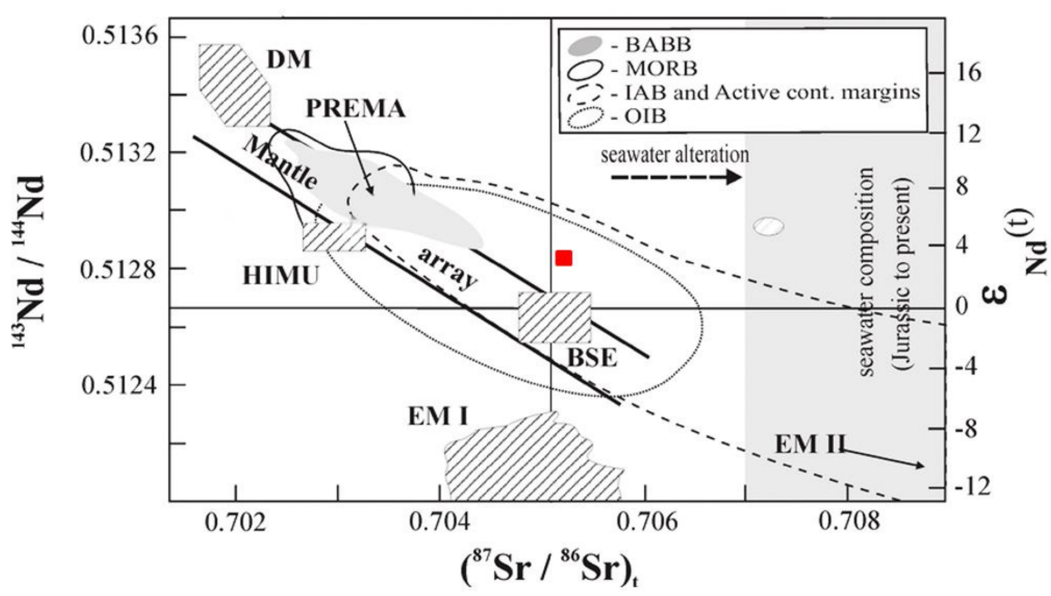

Figure 9. $^{87}Sr/^{86}Sr$ ratio versus $^{143}Nd/^{144}Nd$ isotopic data comparing Oceanic island basalts and MORB sample major reservoirs in the mantle, base diagram from Hofmann (1997) and reference therein. DM - depleted mantle, BSE - bulk silicate Earth, EMI and EMI II -enriched mantle, HIMU - mantle with high U/Pb ratio, PREMA - frequently observed Prevalent Mantle composition. Data for back-arc basin basalts - BABB (gray shaded field) compiled from Wilson (1989) and references therein, Pearce et al. (1995) and Ewart et al. (1998).

indicates that the parental magmas may have undergone some minor degree of crustal contamination.

K/P and Ti/Yb ratios in combination with radiogenic isotope ratios are worthy tools to evaluate the role of contamination (Carlson and Hart, 1987; Leeman and Hawkesworth, 1986; Van Calsteren et al., 1986). The K/P ratio is a good indicator of silicic contamination, since K is enriched and P is depleted in typical upper crust

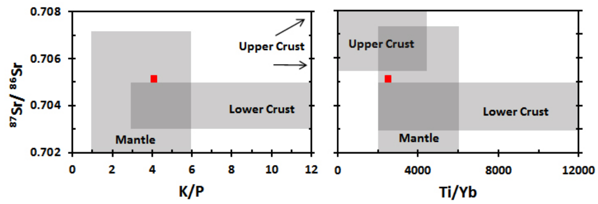

Figure 10. Relationships between Sr isotopic composition and the ratio of Ti/Yb and K/P, which is sensitive to crustal contamination. Fields for common mantle, upper and lower crust (Hart, 1988) and references therein.

(Thompson et al., 1982). The relationship between K/P, Ti/Yb and Sr isotopic composition is presented in Figure 10. The high Nb/U (2.4-11), low Ti/Yb (1600-2600) and low P_2O_5/K_2O (<0.4) ratios propose that the upper crust contamination did not play a major role in their formation (Figure 10).

Nature of mantle source region

Swarm dykes are reported from different geotectonic settings, such as subduction-related (Wang et al., 2020), back-arc extension (Lanjewar et al., 2018), continental extension (Ernst et al., 2019), and post-collisional extension (Long et al., 2020).

Studied samples display 0.72-1.04 wt% TiO_2 (Figure 11), 1-1.9 ppm Nb and 51-69 ppm Zr in their compositions, and suggest similar mantle source. Low Nb/La (0.22-0.44) and high Zr/Nb (36-51) ratios suggest that the samples were not derived from OIB-like asthenospheric mantle, which display ratios Nb/La>1 and Zr/Nb about 5.8 (Bradshaw and Smith, 1994; Smith et al., 1999).

These rocks characterized by low $(Ce/Yb)_N$ values (0.65-1.48) look like N-MORB (Normal Mid-Ocean

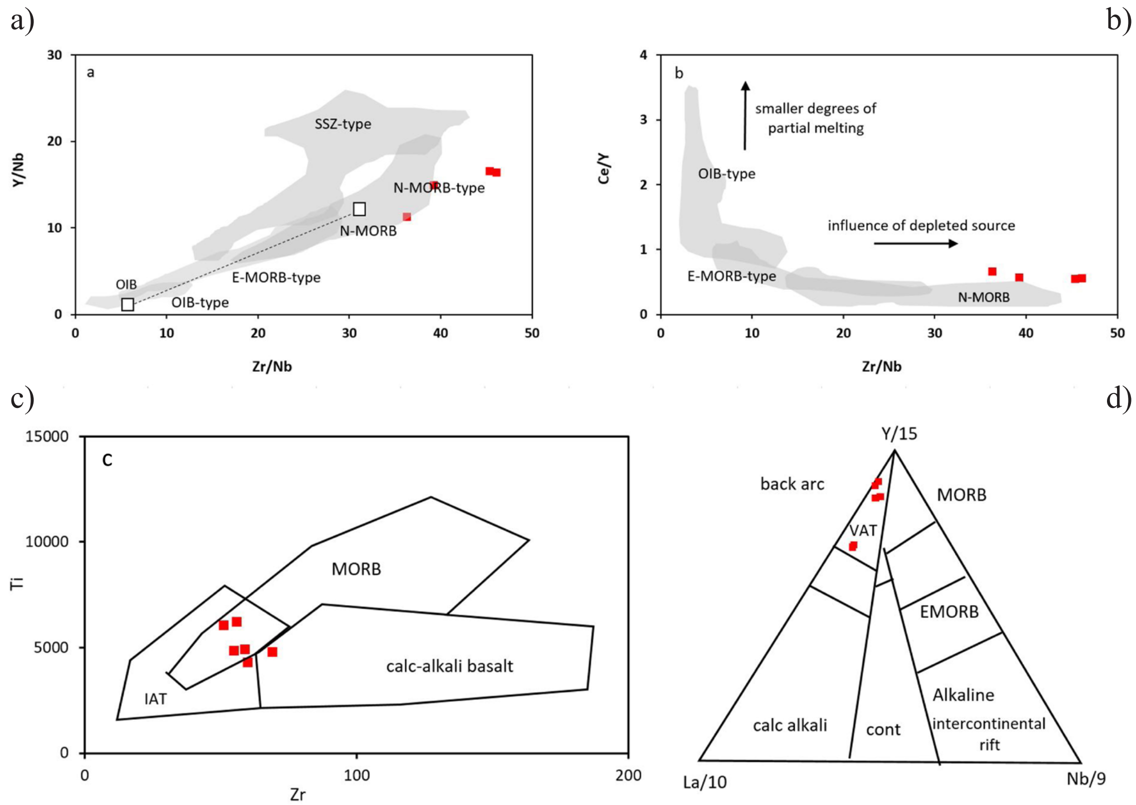

Figure 11. a) Variation of Y/Nb against Zr/Nb for the studied samples. N-MORB and OIB compositions are from Sun and McDonough (1989), b) Variation of Ce/Y against Zr/Nb for the studied samples. N-MORB and OIB compositions are from Sun and McDonough (1989), c) Ti/Zr discrimination diagram (Pearce and Cann, 1973). Samples of studied area plot between volcanic arc and IAT fields, d) Triangular Y/15, La/10, Nb/8 diagram of Cabanis and Lecolle (1989). Samples of studied area plot mainly in volcanic arc field. The abbreviations include MORB: Mid-Ocean ridge basalts; IAT: Island Arc tholeiites.

Ridge Basalt) source (Göncüoglu et al., 2010). Samples were plotted in Y/Nb versus Zr/Nb and Ce/Y versus Zr/Nb diagrams, they are close to N-MORB field and share geochemical features with MORB and IAT (Island Arc Tholeiites) in Zr versus Ti diagram (Figure 11). Based on tectono-magmatic diagrams (Agrawal et al., 2008), these dykes demonstrate IAT affinities (Figure 12). This result was concluded from modification of MORB-like mantle by aqueous fluids and melts coming from subducted oceanic slab (e.g. Gill, 1981; Hawkesworth et al., 1991; Pearce et al., 1995; Göncüoglu et al., 2010). Island arc basalts (IAB) or active continental margin basalts usually show significant enrichment in LILE and LREE like Rb, Ba, K, Th and depletion in Nb, Ta, Zr, and Ti (Scambelluri and Philippot, 2001), but the studied samples show flat REEs distribution with no depletion in Zr and Hf (Figure 6).

Geochemical studies indicate that clinopyroxenes from MORB cumulates have 0.6-1.4 wt% TiO_2, while those from IAT have 0.18-0.54 wt% TiO_2 contents, respectively (Niu et al., 2002; Greene et al., 2006). TiO_2 contents of clinopyroxenes from studied dykes vary from 0.20-0.7 wt% and are comparable to those from IAT cumulates, which were crystallized from a low Ti melt. The generally low Ti content in clinopyroxenes (Table 1) also support the hypothesis that they were crystallized from primary magmas generated from mantle sources, which underwent Ti removal by previous partial melting events (e.g., Hébert and Laurent, 1990).

In addition, variable partial melting of mantle peridotites could results in different TiO2 contents. Mafic magmas derived from lithospheric mantle have lower TiO_2, but usually have higher TiO_2 when derived from asthenospheric mantle (Lightfoot et al., 1993; Ewart et al., 1998). The TiO_2 contents of the studied samples change from 0.72 to 1.04 wt%, lesser than TiO_2 content in OIB (with an average 2.86 wt%), proposing that they could have been derived from lithospheric mantle.

One of the suitable element ratios for providing a melt modeling is the plot of LREE/HREE versus HREE ratio which is an appropriate tool to distinguish between melting the spinel and garnet fields (Baker et al., 1997). The change in La/Yb ratio in spinel-facies melting and melt fraction is smaller compare to mantle source (Figure 13). In contrast, there are large changes in Yb with melt fraction in the garnet-facies (Baker et al., 1997). The studied dykes plot along the batch melting curve of Spinel-lherzolite (Figure 13). Minor changes in Sm/Yb ratios (0.81-1) also indicate the absence of garnet in the mantle source.

Summary Conclusion

Swarm dykes were emplaced in southwest of Jiroft area which is located between ophiolite basins of Nain-Baft and Makran in southeastern Iran. These mafic to intermediate rocks show tholeitic affinity and transitional geochemical characteristics between MORB and island arc tholeiite (IAT) environment, indicating they may have been generated in a back-arc basin.

The back-arc basin in this region is thought to have opened during Late Cretaceous (Arvin and Robinson, 1994) and was closed during Paleocene time

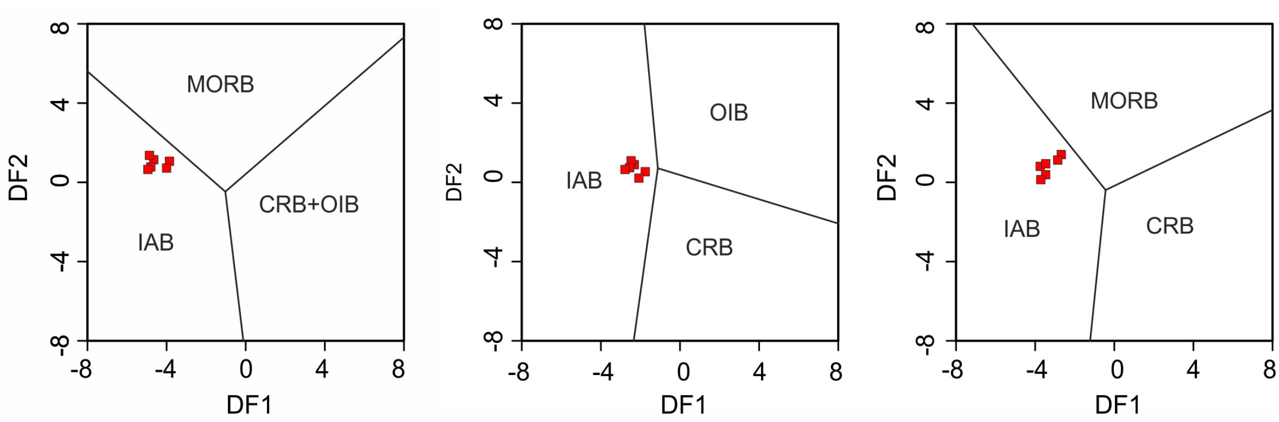

Figure 12. Log transformed immobile trace element tectonic discrimination diagrams, suggesting that the sheeted dykes originated in an island arc tectonic setting (adopted from Agrawal et al., 2008). For diagram (a): DF1 = 0.3518 log (La/Th) + 0.6013 log (Sm/Th) - 1.3450 log (Yb/Th) + 2.1056 log (Nb/Th) - 5.4763; DF2 = -0.3050 log (La/Th) - 1.1801 log (Sm/Th) + 1.6189 log (Yb/Th) + 1.2260 log (Nb/Th) - 0.9944. (b): DF1 = 1.7517 log (Sm/Th) - 1.9508 log (Yb/Th) + 1.9573 log (Nb/Th) - 5.0928; DF2 = -2.2412 log (Sm/Th) + 2.2060 log (Yb/Th) + 1.2481 log (Nb/Th) - 0.8243. (c): DF1 = 0.3305 log (La/Th) + 0.3484 log (Sm/Th) - 0.9562 log (Yb/Th) + 2.0777 log (Nb/Th) - 4.5628; DF2 = -0.1928 log (La/Th) - 1.1989 log (Sm/Th) + 1.7531 log (Yb/Th) + 0.6607 log (Nb/Th) - 0.4384. MORB: Mid-Ocean Ridge Basalts; OIB: Ocean Island Basalts; IAB: Island Arc Basalts and CRB: Continental Rift Basalts.

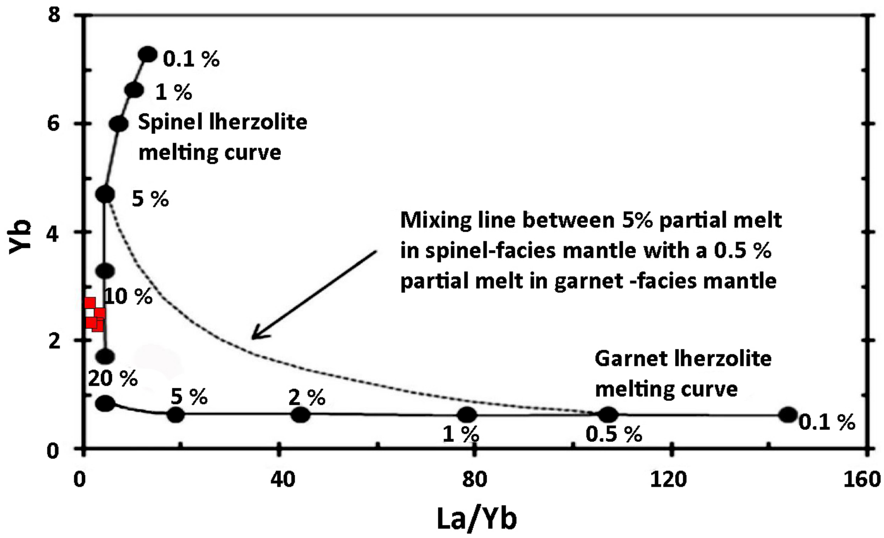

Figure 13. Variation of Yb versus La/Yb for the studied samples compared to non-modal, fractional melting curves for spinel (0.578 Ol, 0.270 Opx, 0.119 Cpx, 0.033 Sp that melts in the proportions 0.10 Ol, 0.27 Opx, 0.50 Cpx, 0.13 Sp) and garnet lherzolite (0.598 Ol, 0.211 Opx; 0.076 Cpx, 0.115 Gt thatmelts in the proportions 0.05 Ol, 0.20 Opx, 0.30 Cpx, 0.45 Gt), and for an upper-crustal estimate taken from Baker et al. (1997).

(Davoudzadeh, 1972; Baroz et al., 1984; Sengör et al., 1988; Arvin and Robinson, 1994; Stampfli and Borel, 2002; Shojaat et al., 2003; Agard, 2011). The U-Pb zircon ages indicate that the dykes were emplaced during the Eocene. The various ages from the inherited zircon crystals in these rocks suggest that substantial crustal basement rocks and Jurassic-Cretaceous magmatism were involved during dyke emplacement. Geochemical and isotopic data indicate they formed by melting of a spinel-mantle source metasomatized by fluids derived from subducted oceanic slab.

ACKNOWLEDGEMENTS

This study is part of the first author's Ph.D. dissertation at Ferdowsi University of Mashhad, Iran.

We are grateful to Dr. Ali Mohammadi for collaborating on age (U-Pb) at the University of Zurich. Thanks to Geological Survey of Iran (GSI), M. Ghoorchi and A. Rajabi for very helpful cooperation.

REFERENCES

Agard P., Omrani J., Jolivet L., Mouthereau F., 2005. Convergence history across Zagros (Iran): constraints from collisional and earlier deformation. International Journal of Earth Sciences 94, 401-419.

Agard P., Omrani J., Jolivet L., Whitechurch H., Vrielynck B., Spakman W., Monié P., Meyer B., Wortel R., 2011. Zagros orogeny: a subduction-dominated process. Geological Magazine 148, 692-725.

Aghazadeh M. and Ojaghi A., 2009. Geological Map, scale 1:25000.

Agrawal S., Guevara M. and Verma S.P., 2008. Tectonic discrimination of basic and ultrabasic volcanic rocks through log-transformed ratios of immobile trace elements. International Geology Review 50, 1057-1079.

Alavi M., 2004. Regional stratigraphy of the Zagros fold-thrust belt of Iran and its proforeland evolution. American Journal of Science 304, 1-20.

Aliani F. and Daraeezadeh Z., 2018. Petrology, geochemistry, and petrogenesis of mafic dykes from the Kermanshah Ophiolite in Sahneh-Harsin area of Western Iran. Geopersia 8, 199-212.

Arvin M. and Robinson P.T., 1994. The petrogenesis and tectonic setting of lavas from the Baft ophiolitic mélange, southwest of Kerman, Iran. Canadian Journal of Earth Sciences 31, 824-834.

Baker J., Menzies M., Thirlwall M., Macpherson C., 1997. Petrogenesis of Quaternary intraplate volcanism, Sana'a, Yemen: implications for plume-lithosphere interaction and polybaric melt hybridization. Journal of Petrology 38, 1359-1390.

Ballato P., Mulch A., Landgraf A., Strecker M.R., Dalconi M.C., Friedrich A., Tabatabaei S.H., 2010. Middle to late Miocene Middle Eastern climate from stable oxygen and carbon isotope data, southern Alborz Mountains, N Iran. Earth and Planetary Science Letters 300, 125-138.

Baroz F., Macaudiere J., Montigny R., Noghreyan M., Ohnenstetter M., Rocci G., 1984. Ophiolites and related formations in the central part of the Sabzevar range (Iran) and possible geotectonic reconstructions. Neues Jahrbuch für

Geologie und Paläontologie -Abhandlungen 168, 358-388.
Bazoobandi M.H., Arian M.A., Emami M.H., Tajbakhsh G.R., Yazdi A., 2015. Geodynamics of Dykes in North of Saveh. Open Journal of Ecology 5, 452-459.
Belousova E.A., Griffi W.L., O'Reilly S.Y., Fisher N.I., 2002. Igneous zircon: trace element composition as an indicator of source rock type. Contribution to Mineralogy and Petrology 143, 602-622.
Berberian F. and Berberian M., 1981, Tectono-plutonic episodes in Iran, Zagros Hindu Kush. Himalaya Geodynamic Evolution 3, 5-32.
Berberian M. and King G.C.P., 1981. Towards a paleogeography and tectonic evolution of Iran. Canadian Journal of Earth Sciences 18, 210-265.
Bradshaw T. and Smith E.I., 1994, Polygenetic Quaternary volcanism at Crater Flat, Nevada. Journal of Volcanology and Geothermal Research 63, 165-182.
Bryan S.E. and Ernst R.E., 2008. Revised definition of large igneous provinces (LIPs). Earth-Science Reviews 86, 175-202.
Bryan S.E. and Ferrari L., 2013. Large igneous provinces and silicic large igneous provinces: Progress in our understanding over the last 25 years. Geological Society of America Bulletin 125, 1053-1078.
Buick I., Storkey A., Williams I.S., 2008. Timing relationships between pegmatite emplacement, metamorphism and deformation during the intra-plate Alice Springs Orogeny, central Australia. Journal of Metamorphic Geology 26, 915-936.
Cabanis B. and Lecolle M., 1989. Le diagramme La/10-Y/15-Nb/8: un outil pour la discrimination des séries volcaniques et la mise en évidence des processus de mélange et/ou de contamination crustale. Comptes rendus de l'Académie des sciences. Série 2, Mécanique, Physique, Chimie, Sciences de l'univers, Sciences de la Terre 309, 2023-2029.
Carlson R.W. and Hart W.K., 1987. Crustal genesis on the Oregon Plateau. Solid Earth 92(B7), 6191-6206.
Chen D.G., Ni T., Xie L.W., 2007. Zircon Lu-Hf isotopic compositions of ultra-high pressure metamorphic rocks from Dabie Terrane, China. Acta Petrologica Sinica 23, 331-342.
Cherniak D.J. and Watson E.B., 2000. Pb diffusion in zircon. Chemical Geology, 172, 5-24.
Cox K.G., 1979. The Interpretation of Igneous Rocks. Allen and Unwin, London, 450 pp.
Davoudzadeh M., 1972. Geology and petrography of the area north of Nain, central Iran. Report, Geological Survey of Iran, Tehran, 89 pp. (in Persian).
Ernst R.E. and Buchan K.L., 2001. The use of mafic dyke swarms in identifying and locating mantle plumes. Mantle plumes: Their identification through time 352, 247-265.
Ernst R.E., 2014. Large Igneous Provinces. Cambridge University Press, 666 pp.
Ernst, R.E., Liikane, D.A., Jowitt, S.M., Buchan, K.L. and Blanchard, J.A., 2019. A new plumbing system framework for mantle plume-related continental Large Igneous Provinces and their mafic-ultramafic intrusions. Journal of Volcanology and Geothermal Research 384, 75-84.
Ewart A., Collerson K.D., Regelous M., Wendt J.I., Niu Y., 1998. Geochemical Evolution within the Tonga-Kermadec-Lau Arc-Back-arc System: the Role of Varying Mantle Wedge Composition in Space and Time. Journal of Petrology 39, 331-368.
Gill J.B., 1981. Orogenic Andesites and Plate Tectonics. Springer-Verlag, Berlin, 358 pp.
Göncüoglu M.C., Sayit K., Tekin U.K., 2010. Oceanization of the northern Neotethys: geochemical evidence from ophiolitic melange basalts within the Izmir-Ankara suture belt, NW Turkey. Lithos 116, 175-187.
Greene A.R., DeBari S.M., Kelemen P.B., Blusztajn J., Clift P.D., 2006. A detailed geochemical study of island arc crust: the Talkeetna arc section, south-central Alaska. Journal of Petrology 47, 1051-1093.
Hart S.R., 1984. A large-scale isotope anomaly in the Southern Hemisphere mantle. Nature 309 (5971), 753-757.
Hawkesworth C.J., Hergt J.M., Ellam R.M., McDermott F., 1991. Element fluxes associated with subduction related magmatism. Philosophical Transactions of the Royal Society 335, 393- 405.
Hébert R. and Laurent R., 1990. Mineral chemistry of the plutonic section of the Troodos ophiolite: new constraints for genesis of arc-related ophiolites. In Troodos 1987. Symposium 149-163.
Iljina M. and Hanski E., 2005. Layered mafic intrusions of the Tornio-Na¨ra¨nka¨vaara belt. In: Developments in Precambrian Geology. (Eds.): P.A.N.M. Lehtinen and O.T. Rämö, Elsevier, Amsterdam, 101-137.
Jahangiri H., Saadat S., Mazaheri S.A., Heidarian Shahri M.R., Foudazi M., Omrani J., 2020. The middle Jurassic-Early Cretaceous pillow and massive lava flows associated with pelagic sediments in the Ghaleh-Rigi area, southern east of Iran: age and geochemistry. Geopersia, doi: 10.22059/geope.2019.278194.648471.
James R.S., Easton R.M., Peck D.C., Hrominchuk J.L., 2002. The East Bull Lake intrusive suite: remnants of a2 48 Ga large igneous and metallogenic province in the Sudbury area of the Canadian Shield. Economic Geology 97, 1577-1606.
Kerr A.C., White R.V., Saunders A.D., 2000. LIP reading: Recognizing oceanic plateaux in the geological record. Journal of Petrology 41, 1041-1056.
Koschek G., 1993. Origin and significance of the SEM cathodoluminescence from zircon. Journal of Microscopy 171, 223-232.
Lanjewar S. and Randive K., 2018. Lamprophyres from the Harohalli dyke swarm in the Halaguru and Mysore areas, Southern India: Implications for backarc basin magmatism. Journal of Asian Earth Sciences 157, 329-347.

Leeman W.P. and Hawkesworth C.J., 1986. Open magmatic systems, some isotopic and trace element constraints. Journal of Geophysical Research 91, 5901-5912.

Lightfoot P., Hawkesworth C., Hergt J., Naldrett A., Gorbachev N.S., Fedorenko V.A., Doherty W., 1993, Remobilisation of the continental lithosphere by a mantle plume: Major, trace-element, and Sr-Nd and Pb isotope evidence from picritic and tholeiitic lavas of the Noril'sk District, Siberian Trap, Russia. Contributions to Mineralogy and Petrology 114, 171-188.

Long X., Wu B., Sun M., Yuan C., Xiao W., Zuo R., 2020. Geochronology and geochemistry of Late Carboniferous dykes in the Aqishan-Yamansu belt, eastern Tianshan: Evidence for a post-collisional slab breakoff. Geoscience Frontiers 11, 347-362.

McDonough W.F. and Sun S.S., 1995. The composition of the Earth. Chemical geology 120, 223-253.

Middlemost Eric A.K., 1994. Naming materials in the magma/igneous rock system. Earth-Science Reviews 37, 215-224.

Mikova J. and Denkova P., 2007. Modified chromatographic separation scheme for Sr and Nd isotope analysis in geological silicate samples. Journal of Geosciences 52, 221-226.

Miyashiro A., 1974. Volcanic rock series in island arcs and active continental margins. American Journal of Science 274, 321-355.

Mohajjel M. and Fergusson C.L., 2014. Jurassic to Cenozoic tectonics of the Zagros Orogen in northwestern Iran. International Geology Review 56, 263-287.

Mohajjel M., Fergusson C.L., Sahandi M.R., 2003. Cretaceous-Tertiary convergence and continental collision, Sanandaj-Sirjan zone, western Iran. Journal of Asian Earth Sciences 21, 397-412.

Mohr P., 1987. Patterns of faulting in the Ethiopian Rift Valley. Tectonophysics 143, 169-179.

Niu Y., Gilmore T., Mackie S., Greig A., Bach W., 2002. Mineral chemistry, whole-rock compositions, and petrogenesis of Leg 176 gabbros: data and discussion. In: Proceedings of the Ocean Drilling Program, scientific results 176, 1-60. College Station, TX: Ocean Drilling Program.

Pearce J.A. and Cann J.R., 1973. Tectonic setting of basic volcanic rocks determined using trace element analyses. Earth and Planetary Science Letters 19, 290-300.

Pearce J.A., Baker P.E., Harvey P.K., Luff I.W., 1995. Geochemical evidence for subduction flukses, mantle melting for fractional crystalization beneath the South Sandwich Island Arc. Journal of Petrology 36, 1073-1109.

Peck D.C., Keays R.R., James R.S., Chubb P.T., Reeves S.J., 2001. Controls on the formation of contact-type platinum-group element mineralization in the East Bull Lake intrusion. Economic Geology 96, 559-581.

Pin C. and Zalduegui J.S., 1997. Sequential separation of light rare-earth elements, thorium and uranium by miniaturized extraction chromatography: application to isotopic analyses of silicate rocks. Analytica Chimica Acta 339, 79-89.

Pirnia T., Saccani E., Torabi G., Chiari M., Gorican S., Barbero E., 2020. Cretaceous tectonic evolution of the Neo-Tethys in Central Iran: Evidence from petrology and age of the Nain-Ashin ophiolitic basalts. Geoscience Frontiers 11, 57-81.

Rubatto D., 2002. Zircon trace element geochemistry: portioning with garnet and the link between U-Pb ages and metamorphism. Chemical Geology 184, 123 -138.

Sadeghi S. and Yassaghi A., 2015. Spatial evolution of Zagros collision zone in Kurdistan-NW Iran, constraints for Arabia-Eurasia oblique convergence. Solid Earth Discussions 7, 2735-2773.

Scambelluri M. and Philippot P., 2001, Deep fluids in subduction zones. Lithos 55, 213-227.

Sengör A.M.C., Altıner D., Cin A., Ustaömer T., Hsü K.J., 1988. Origin and assembly of the Tethyside orogenic collage at the expense of Gondwana Land. Geological Society, London, Special Publications 37, 119-181.

Shand S.J., 1943. The eruptive rocks. John Wiley, New York, 444 pp.

Shojaat B., Hassanipak A.A., Mobasher K., Ghazi A.M., 2003. Petrology, geochemistry and tectonics of the Sabzevar ophiolite, North Central Iran. Journal of Asian Earth Sciences 21, 1053-1067.

Smith E.I., Sanchez A., Walker J.D. and Wang K., 1999. Geochemistry of mafic magmas in the Hurricane Volcanic Field, Utah: Implications for small and large scale chemical variability of the Lithospheric Mantle. Journal of Geology 107, 433-448.

Stampfli G.M. and Borel G.D., 2002. A plate tectonic model for the Paleozoic and Mesozoic constrained by dynamic plate boundaries and restored synthetic oceanic isochrons. Earth and Planetary Science Letters 196, 17-33.

Stöcklin J., 1968. Structural history and tectonics of Iran: a review. American Association of Petroleum Geologists 52, 1229-1258.

Stöcklin J., 1977. Structural correlation of the Alpine ranges between Iran and central Asia. Mémoires de la Société géologique de France 8, 333-353.

Sun S.S. and McDonough W.F., 1989. Chemical and isotopic systematics of oceanic basalts: implications for mantle composition and processes. In: Magmatism in the Ocean Basins. (Eds.): A.D. Saunders and M.J. Norry, Geological Society, London, Special Publications 42, 313-345.

Tanaka T., Togashi S., Kamioka H., Amakawa H., Kagami H., Hamamoto T., Yuhara M., Orihashi Y., Yoneda S., Shimizu H., Kunimaru T., Takahashi K., Yanagi T., Nakano T., Fujimaki H., Shinjo R., Asahara Y., Tanimizu M., Dragusanu C., 2000. JNdi-1: A neodymium isotopic reference in consistency with LaJolla neodymium. Chemical Geology 168, 279-281.

Thompson R.N., Dickin A.P., Gibson I.L., Morrison M.A., 1982. Elemental fingerprints of isotopic contamination of Hebridean Palaeocene mantle-derived magmas by Archaean sial. Contributions to Mineralogy and Petrology 79, 159-168.

Van Calsteren P.W.C., Harris N.B.W., Hawkesworth C.J., Menzies M.A., Rogers N.W., 1986. Xenoliths from southern Africa: a perspective on the lower crust. Geological Society, London, Special Publication 24, 351-362.

Vincent S.J., Allen M.B., Ismail-Zadeh A.D., Flecker R., Foland K.A., Simmons M.D., 2005. Insights from the Talysh of Azerbaijan into the Paleogene evolution of the South Caspian region. Geological Society of America Bulletin 117, 1513-1533.

Wang X., Wang Z., Cheng H., Foley S., Xiong L., Hu Z., 2020. Early cretaceous lamprophyre dyke swarms in Jiaodong Peninsula, eastern North China Craton, and implications for mantle metasomatism related to subduction. Lithos 368-369, https://doi.org/10.1016/j.lithos.2020.105593.

Wheeler R.S., Browne P.R.L., Rodgers K.A., 2001. Iron-rich and iron-poor prehnites from the Way Linggo epithermal Au-Ag deposit, southwest Sumatra, and the Heber geothermal field, California. Mineralogical Magazine 65, 397-406.

Whitney D.L. and Evans B.W., 2010. Abbreviations for names of rock-forming minerals. American mineralogist 95, 185-187.

Wilson M., 1989. Igneous petrogenesis a global tectonic approach. Department of earth Science (2nd edition), Springer Netherlands, 466 pp.

Wu Y.B., Zheng Y.F., Zhang S.B., Zhao Z.F., Wu F.Y., Liu X.M., 2007. Zircon U-Pb ages and Hf isotope compositions of migmatite from the North Dabie terrane in China: constraints on partial melting. Journal of Metamorphic Geology 25, 991-1009.

Zhai Q.G., Li C., Wang J., Zhan Sheng J., Wang Y., 2009. SHRIMP U-Pb dating and Hf isotopic analyses of zircons from the mafic dyke swarms in central Qiangtang area, Northern Tibet. Chinese Science Bulletin 54, 2279-2285.